TU Delft

Delft University of Technology

The high-temperature heat capacity of the $(Th,U)O_2$ and $(U,Pu)O_2$ solid solutions

Valu, S.O.; Beneš, O.; Manara, D; Konings, R. J.M.; Cooper, M. W.D.; Grimes, R. W.; Guéneau, C

DOI
10.1016/j.jnucmat.2016.11.010

Publication date
2017

Document Version
Final published version

Published in
Journal of Nuclear Materials

Citation (APA)
Valu, S. O., Beneš, O., Manara, D., Konings, R. J. M., Cooper, M. W. D., Grimes, R. W., & Guéneau, C. (2017). The high-temperature heat capacity of the $(Th,U)O_2$ and $(U,Pu)O_2$ solid solutions. *Journal of Nuclear Materials*, *484*, 1-6. https://doi.org/10.1016/j.jnucmat.2016.11.010

Important note
To cite this publication, please use the final published version (if applicable).
Please check the document version above.

Copyright
Other than for strictly personal use, it is not permitted to download, forward or distribute the text or part of it, without the consent of the author(s) and/or copyright holder(s), unless the work is under an open content license such as Creative Commons.

Takedown policy
Please contact us and provide details if you believe this document breaches copyrights.
We will remove access to the work immediately and investigate your claim.

This work is downloaded from Delft University of Technology.
For technical reasons the number of authors shown on this cover page is limited to a maximum of 10.

Journal of Nuclear Materials 484 (2017) 1–6

Contents lists available at ScienceDirect

Journal of Nuclear Materials

journal homepage: www.elsevier.com/locate/jnucmat

The high-temperature heat capacity of the $(Th,U)O_2$ and $(U,Pu)O_2$ solid solutions

S.O. Vălu [a, b], O. Beneš [a], D. Manara [a], R.J.M. Konings [a, b, *], M.W.D. Cooper [c, d], R.W. Grimes [c], C. Guéneau [e]

[a] European Commission, Joint Research Centre, P.O. Box 2340, 76125 Karlsruhe, Germany
[b] Delft University of Technology, Faculty of Applied Physics, Mekelweg 15, 2629 JB Delft, The Netherlands
[c] Department of Materials, Imperial College, London, SW7 2AZ, UK
[d] Materials Science and Technology Division, Los Alamos Laboratory, P.O. Box 1663, Los Alamos, NM 87545, USA
[e] CEA, DANS, DPC, SCCME, LM2T, Centre de Saclay, Gif-sur-Yvette Cedex, France

ARTICLE INFO

Article history:
Received 5 February 2016
Received in revised form
28 October 2016
Accepted 7 November 2016
Available online 9 November 2016

Keywords:
Actinide mixed oxides
Calorimetry
Heat capacity

ABSTRACT

The enthalpy increment data for the $(Th,U)O_2$ and $(U,Pu)O_2$ solid solutions are reviewed and complemented with new experimental data (400–1773 K) and many-body potential model simulations. The results of the review show that from room temperature up to about 2000 K the enthalpy data are in agreement with the additivity rule (Neumann-Kopp) in the whole composition range. Above 2000 K the effect of Oxygen Frenkel Pair (OFP) formation leads to an excess enthalpy (heat capacity) that is modeled using the enthalpy and entropy of OFP formation from the end-members. A good agreement with existing experimental work is observed, and a reasonable agreement with the results of the many-body potential model, which indicate the presence of the diffuse Bredig (superionic) transition that is not found in the experimental enthalpy increment data.

© 2016 Published by Elsevier B.V.

1. Introduction

The heat capacity of a material is an important thermodynamic property describing the relation between heat and temperature, and is therefore of crucial importance for materials engineering. Heat capacity itself is strongly temperature dependent, and this dependence can be well described by the phonon structure of a solid, which represents the vibrational motions in the crystal as collective oscillations. According to Debye theory, the heat capacity of a perfect crystal is zero at the absolute zero of temperature, since no motion exists, and approaches the Dulong-Petit limit $3NR$ at high temperature, where N is the number of moles of atoms and R is the universal gas constant. In real crystals, however, the effect of electronic contributions and anharmonicity due to lattice imperfections must also be taken into account.

In view of this, the temperature dependence of the heat capacity of refractory ceramic materials can be divided in three regions: (a) the low temperature region in which the heat capacity rapidly rises to reach the Dulong-Petit limit, (b) the intermediate region in which the heat capacity is approximately constant and close to the Dulong-Petit limit, and (c) the high temperature region in which anharmonicity effects due to the contribution of lattice thermal defects cause an excess contribution. As an example, Fig. 1 shows the heat capacity of ThO_2, which reaches the Dulong-Petit limit around 500 K and exhibits a strong increase above 2000 K, which has been attributed to Oxygen Frenkel Pair (OFP) formation [1]. The same effects have been observed for other fluorite structured actinide dioxides, such as UO_2 and PuO_2 [1].

The heat capacity of solid solutions has the same temperature dependence, but due to the mixing of atoms on the lattice sites, the effect of impurity-phonon scattering has to be considered, which is highly dependent on the differences in the mass and size of the substitutional atoms. This effect was very clearly observed in the solid solutions of the lanthanide phosphates with monazite structure [2], which revealed an increasing excess enthalpy with increasing difference in the ionic radius of the lanthanides. In the absence of such strain effects, the heat capacity of solid solutions can be described well by the Neumann-Kopp rule, which states that it is the weighted average of the end members.

* Corresponding author. European Commission, Joint Research Centre, P.O. Box 2340, 76125 Karlsruhe, Germany.
E-mail address: rudy.konings@ec.europa.eu (R.J.M. Konings).

http://dx.doi.org/10.1016/j.jnucmat.2016.11.010
0022-3115/© 2016 Published by Elsevier B.V.

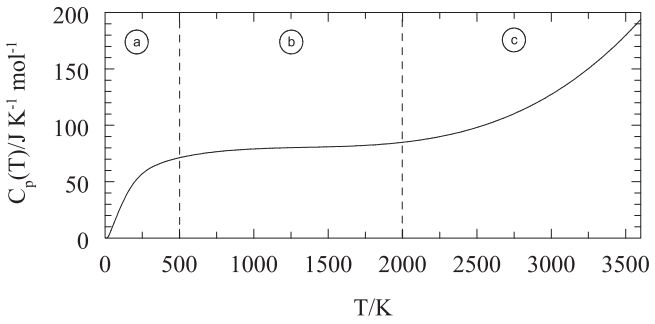

Fig. 1. The heat capacity of ThO_2 from 0 K to the melting point showing the three typical temperature regions: (a) the low temperature region in which the heat capacity rapidly rises to reach the Dulong-Petit limit, (b) the intermediate region in which the heat capacity is approximately constant and close to the Dulong-Petit limit, and (c) the high temperature region in which anharmonicity effects due to the contribution of lattice thermal defects cause an excess contribution. The graph is based on the recommended data by Konings et al. [8], obtained by an assessment of experimental enthalpy increment and heat capacity data.

In our studies of the actinide dioxides solutions we are addressing these issues with the goal to obtain a detailed predictive understanding of the heat capacity and other thermodynamic quantities over a wide temperature range. In this paper we will examine the $(Th,U)O_2$ and $(U,Pu)O_2$ solid solutions in detail. First we will present enthalpy drop calorimetric measurements to examine whether the mixed oxide solid solution exhibits impurity-phonon scattering (lattice strain) effects or follows the Neumann-Kopp rule, and second we will use the model for the OFP contribution to the heat capacity that we have applied to the actinide dioxides [1], to describe the high temperature heat capacity of the mixed oxide solid solution and compare the results to literature data. Finally comparison will be made to molecular dynamics calculations employing a many-body potential recently developed by Cooper-Rushton-Grimes (CRG) for a range of actinide oxides and their solid solutions [3–5].

2. The intermediate temperature region: checking the Neumann-Kopp rule

Enthalpy increments for $(Th,U)O_2$ samples (about 100 mg) with 20, 40 and 60 mol% uranium were measured using a Setaram MHTC-96 calorimeter operating in drop mode, the maximum operating temperature of which is 1773 K, using a constant gas flow of helium (see Ref. [6] for details on the operation and calibration procedures). The standard deviation of the multiple drops at each temperature was between 3 and 6%. The samples were prepared from aqueous solutions using a gel-supported precipitation route, followed by sintering to produce dense pellets. The U/(Th + U) composition was derived from the analysis of the metal concentrations in the starting solution (thorium nitrate and uranyl nitrate, respectively). The materials were analyses by X-Ray powder diffraction (XRD), confirming that they were single phase materials. The measured lattice parameters (Table 1) agreed with those expected for these compositions assuming a Vegard's law interpolation between the end-members, consistent with the observations of Hubert et al. [7] and the calculations by Cooper et al. [4], confirming that the oxygen-to-metal ratio is 1.99 ± 0.01.

The results for the three compositions of the $(Th,U)O_2$ solid solution have been compared to the results for ideal behaviour (i.e. complying with the molar additivity rule (Neumann-Kopp)), and the difference is shown in Fig. 2. The data for the end-member have been taken form a recent critical review [8]. It is clear that our results are in fair to good agreement with the additivity rule, the difference being on the order of ±6%. It should be noted that the absolute error is relatively large, as the difference values are a small number calculated from three much larger numbers (the experimental value and the values for the two end-members), and is not shown in the graphs.

Enthalpy increments for the compositions $(Th_{0.90}U_{0.10})O_2$, $(Th_{0.50}U_{0.50})O_2$ and $(Th_{0.10}U_{0.90})O_2$ have also been reported by Anthonysamy et al. [9] and Kandan et al. [10] in the temperature range 400–800 K. Their results, analysed in a similar manner, are also shown in Fig. 2 and also reveal no measurable deviation from the additivity rule, the uncertainty being approximately a factor two to three smaller than our results. Thus it is clear that the enthalpy increment and therefore also the heat capacity of the $(Th,U)O_2$ solid solution can be described satisfactorily by the Neumann-Kopp rule in this temperature range, confirming the conclusions from Anthonysamy et al. [9] and Kandan et al. [10].

Similarly, a comparison to the Neumann-Kopp additivity rule has been made for the $(U,Pu)O_2$ solid solution. $(U,Pu)O_2$ samples with 25, 50, 75, 80 and 90 mol% plutonium were also prepared using the gel-supported precipitation route and details are reported in Refs. [11,12]. The lattice parameters determined by XRD are consistent with Vegards's law [13] and the calculations by Cooper et al. [4], and suggest that the oxygen-to-metal ratio is 2.00 ± 0.01 (Table 1).

The results for the comparison of our results with the molar additivity rule (Neumann-Kopp) for the five compositions measured in this study are shown in Fig. 3 together with those reported by Gibby [14] and Kandan et al. [15,16]. Similar to the $(Th,U)O_2$ solid solution, we do not find any evidence for deviation from the additivity rule in the experimental values for the $(U,Pu)O_2$ solid solution. Again, the spread in the our results is a factor of two to three above the other studies.

3. The high temperature region: modeling the OFP contribution

In a recent paper [1] we applied the theoretical model proposed

Table 1
Characteristics of the samples used for calorimetric measurements.

Sample composition	Synthesis Technique[a]	Lattice parameter/nm	O/M	reference
$Th_{0.60}\ U_{0.20}\ O_2$	GSP	555.01(2)	1.99 ± 0.01	[12]
$Th_{0.40}\ U_{0.40}\ O_2$	GSP	552.43(2)	1.99 ± 0.01	[12]
$Th_{0.20}\ U_{0.60}\ O_2$	GSP	549.85(2)	1.99 ± 0.01	[12]
$U_{0.75}\ Pu_{0.25}\ O_2$	GSP	545.45(2)	1.99 ± 0.01[b]	[11]
$U_{0.50}\ Pu_{0.50}\ O_2$	GSP	543.77(2)	1.99 ± 0.01[b]	[11]
$U_{0.75}\ Pu_{0.25}\ O_2$	GSP	541.5(3)	1.99 ± 0.01	[11]
$U_{0.20}\ Pu_{0.80}\ O_2$	infiltration	540.77(3)	2.00 ± 0.01	[11]
$U_{0.10}\ Pu_{0.90}\ O_2$	infiltration	540.37(2)	2.01 ± 0.01	[11]

[a] GSP, gel-supported precipitation.
[b] Confirmed by XANES analysis [12].

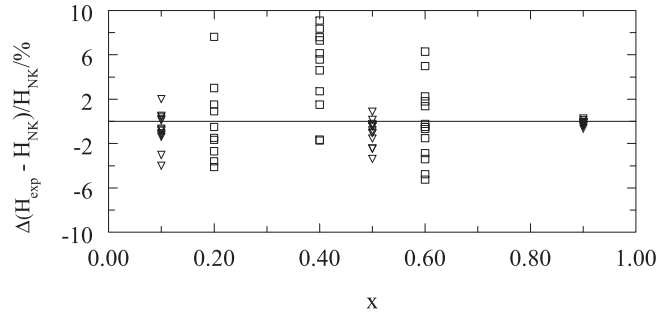

Fig. 2. The difference between the experimental enthalpy increment data for $(Th_{1-x}U_x)O_2$ and the Neumann-Kopp additivity rule; □, the results of the current study; △ from Anthonysamy et al. [9], ▽ the results from Kandan et al. [10].

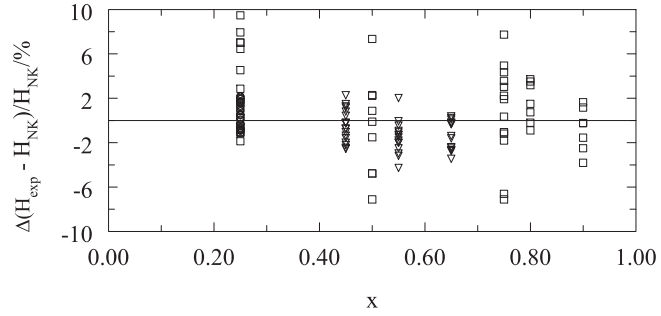

Fig. 3. The difference between the experimental enthalpy increment data for $(U_{1-x}Pu_x)O_2$ and the Neumann-Kopp additivity rule; □, the results of the current study; ▽ and △ the results from Kandan et al. [15,16]; ○ from Gibby [14].

by Szwarc [17] to analyse the defect contribution to the high-temperature excess enthalpy of the actinide dioxides above about 2000 K. This model, which is based on the statistical thermodynamic approach developed by Wagner and Schottky [18], describes the excess heat capacity in terms of the energetics of the Oxygen Frenkel pair (OFP) formation, and was preferred to empirical description as for example, used in Ref. [19]. The excess heat capacity is given by the equation:

$$C_{p,exc} = \frac{\Delta H_{OFP}^2}{\sqrt{2}\mathbf{R}T^2}\exp\left(\frac{-\Delta H_{OFP}}{2\mathbf{R}T}\right)\exp\left(\frac{\Delta S_{OFP}}{2\mathbf{R}}\right) \quad (1)$$

where ΔH_{OFP} and ΔS_{OFP} are the enthalpy and entropy of oxygen Frenkel pair formation, **R** is the universal gas constant, and T is the absolute temperature. By fitting the excess heat capacity for ThO_2, UO_2 and PuO_2, derived from experimental heat capacity and enthalpy increment data, we could derive ΔH_{OFP} and ΔS_{OFP} for these compounds, and the enthalpy values ΔH_{OFP} for were found to be in good agreement with existing literature values from experiments and theoretical data [1,20]. Particularly a substantial number of Density Functional Theory (DFT) and Molecular Dynamics (MD) studies have reported for UO_2 and the recent state-of-the-art DFT/LDA + U [21] and MD [22] studies, not included in the discussion in Ref. [1], give further confirmation.

The excess heat capacity caused by OFP formation appeared to start at progressively lower temperature with increasing atomic number of the actinide ion, reflected by a decreasing ΔH_{OFP}. In this analysis the eventual Bredig (superionic) transition in these compounds, related to oxygen Frenkel pair disorder, is neglected because the enthalpy increment data on which our analysis is based, do not reveal evidence for it. This transition has been reported for UO_2 by Hiernaut et al. [23] and for ThO_2 by Ronchi and Hiernaut [24] and has been explained by order-disorder displacement at the anion site, and is thus closely related to OFP formation. We will discuss this further in the next sections.

For the $(Th,U)O_2$ solid solution we have applied an interpolation for the ΔH_{OFP} and ΔS_{OFP} values assuming an ideal mixing behaviour, as shown in the equations below:

$$\Delta H_{OFP}^{ss} = x \times \Delta H_{OFP}^{ThO_2} + (1-x) \times \Delta H_{OFP}^{UO_2} \quad (2)$$

$$\Delta S_{OFP}^{ss} = x \times \Delta S_{OFP}^{ThO_2} + (1-x) \times \Delta S_{OFP}^{UO_2} \quad (3)$$

The results for three compositions of the $(Th_{1-x}U_x)O_2$ solution thus obtained from the lattice contributions and the excess contributions from eq. (1) are shown in Fig. 4, in a plot of the apparent heat capacity of reduced enthalpy increment $\{H^\circ(T) - H^\circ(298.15\ K)\}/(T - 298.15)$, which is a highly sensitive function. The compositions were chosen such that they can be compared to the experimental enthalpy increment data from 2300 to 3400 K as reported by Fischer et al. [25]. To enable this comparison, we have to estimate the lattice heat capacity of the solid solution. This was done by applying the Neumann-Kopp rule to the lattice contributions considered in our work on the actinide dioxides [1], in line with the results presented in the previous section. The agreement for the highest U concentration $(Th_{0.70}U_{0.30})O_2$ is excellent, confirming that a consistent model for the end-members and the solid solution has been obtained. This is further confirmed by comparison to the results for the $(Th_{0.85}U_{0.15})O_2$ composition for which the enthalpy increments were also measured by Fischer et al. [25], also shown in Fig. 4. Unfortunately the experimental results for the $(Th_{0.92}U_{0.08})O_2$ composition by Fischer et al. do not fit the calculations that well, the values being even below the ThO_2 curve, as already noted by the authors [25]. It should be noted that this sample was fabricated in a different laboratory, compared to the other two samples, and the deviation could be explained by an incorrect oxygen-to-metal ratio determination for this case.

Similarly, the reduced enthalpy increment of the $(U_{0.80}Pu_{0.20})O_2$ composition has been calculated from the ΔH_{OFP} and ΔS_{OFP} values for the end members and compared to the experimental results by Ogard [26] for samples with stoichiometry O/(U + Pu) = 2.00 and 1.98. Fig. 5 shows that an excellent agreement exists between the experimental and calculated results in the complete temperature range of the measurements, confirming our approach. Also shown are the results by Leibowitz et al. [27] for a $(U_{0.80}Pu_{0.20})O_2$ sample with O/(U + Pu) = 1.97, which are slightly lower than those by Ogard. The overall trend in these results may suggests that the energetics of formation and/or annihilation of OFP's in these compounds change with the concentration of the oxygen vacancies in the structure.

This approach yields heat capacity values which are close to those obtained from the NK interpolation to about 2000 K, above that temperature the results obtained by Szwarc's model for oxygen Frenkel pair formation (OPF) are systematically lower, up to 4 $J \cdot K^{-1} \cdot mol^{-1}$ for $(Th_{0.70}U_{0.30})O_2$ and 6 $J \cdot K^{-1} \cdot mol^{-1}$ for $(U_{0.80}Pu_{0.20})O_2$, which is due to the non-linear nature of equation (1).

4. The high temperature region: comparison to many-body potential model calculations

Cooper-Rushton-Grimes (CRG) [3,4] developed a many-body potential model for describing a range of thermophysical properties of actinide dioxides and their solid solutions, including heat capacity. It is interesting to compare the enthalpy increment data obtained by that approach to the $(Th_{1-x}U_x)O_2$ and $(U_{0.80}\ Pu_{0.20})O_2$

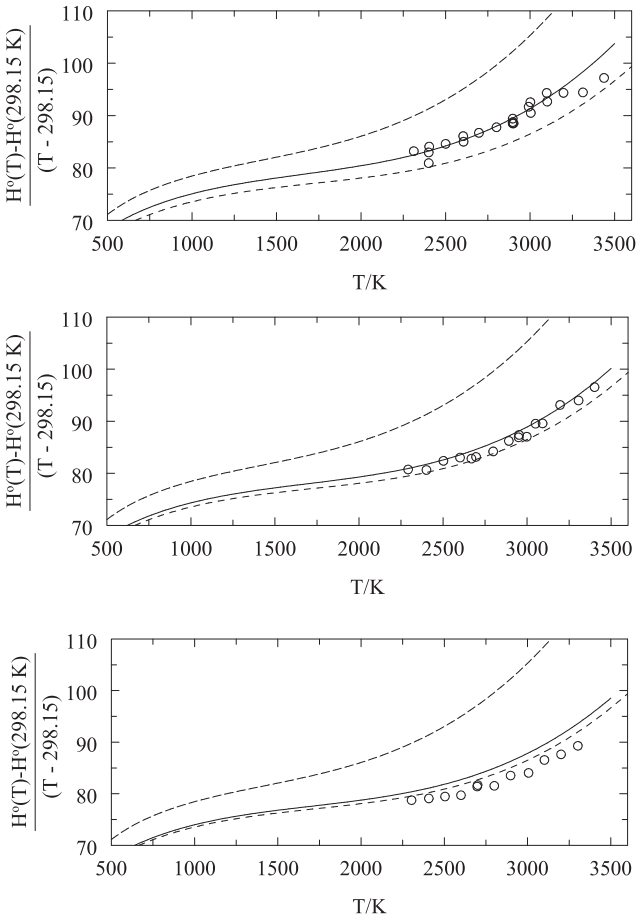

Fig. 4. The reduced enthalpy increment (in J K^{-1} mol^{-1}) of $(Th_{0.70}U_{0.30})O_2$ (top), $(Th_{0.85}U_{0.15})O_2$ (middle) and $(Th_{0.92}U_{0.08})O_2$ (bottom); the solid lines represent the results of the calculation based on the Szwarc model presented in this work; the symbols show the experimental data from Fischer et al. [25]; the dashed lines show the curves for the end members ThO_2 and UO_2.

compositions extensively discussed in the previous section. Therefore additional molecular dynamics simulations were carried out using the LAMMPS [28] code in conjunction with this many-body potential [3–5]. The model describes pairwise interactions using a conventional short range Buckingham-Morse potential [29,30] with long range electrostatic forces calculated using the Ewald method [31] with the Particle-Particle Particle-Mesh (PPPM) implementation [32]. In addition to the pairwise description, many-body effects are incorporated using the embedded atom method (EAM) of Daw and Baskes [33] in a way that modulates the interactions such that each bond becomes progressively weaker as the coordination of a given atom is increased [34]. Consequently, the potential was able to reproduce a wide range to thermophysical properties from 300 K to 3000 K. The parameters developed for the mixed oxide systems are given in Refs. [3,4] for $(U,Th)O_2$ and [4,5] $(U,Pu)O_2$, respectively. Note also that the $(U,Pu)O_2$ parameters were modified [5] from the original potential set [3] to enable the PuO_2 melting point to be more accurately reproduced. Solid solution structures for $(U_{0.80}Pu_{0.20})O_2$, $(Th_{0.70}U_{0.30})O_2$, $(Th_{0.85}\ Pu_{0.15})O_2$ and $(Th_{0.92}U_{0.08})O_2$ were generated by randomly assigning U^{4+}, Pu^{4+} and Th^{4+} cations across the 4a Wyckoff sites (fluorite actinide sites) throughout a 10 × 10 × 10 fluorite unit cell. Stoichiometry was maintained throughout, such that the metal to oxygen ratio is always 2. These systems were equilibrated at zero pressures and a range of temperatures for 20 ps in the NPT ensemble using thermostat and barostat relaxation times of 0.1 ps and 0.5 ps respectively. Over the final 4ps of equilibration the enthalpy of the system was averaged. This was repeated for temperatures ranging from 300 K to 3600 K (ThO_2 melting point) at 25 K intervals. For each composition this procedure was repeated for 10 randomly generated structures.

The results, also expressed as reduced enthalpy increment, are shown in Fig. 6 and can be compared to the experimental results in Figs. 4 and 5. It can be observed that the computational results for the $(Th_{1-x}\ U_x)O_2$ solid solution are in reasonable agreement with the experimental results and the estimates based on the OFP model described in the previous section. In the lower temperature range the CRG model slightly overestimates the reduced enthalpy increment, and thus the heat capacity, and in the mid range the agreement is very good, also confirming that the additivity rule (Neumann-Kopp) is followed. The most striking difference occurs in the high temperature region, for which the CRG calculations show an anomaly that is related to the diffuse Bredig transition predicted for all three compositions, which is not present in the OFP model, nor in the experimental enthalpy data.

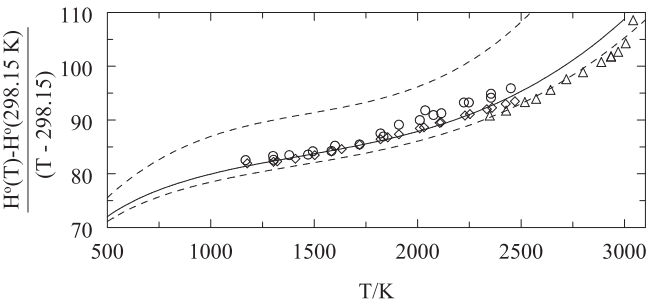

Fig. 5. The reduced enthalpy increment (in J• $K•^{-1}$ mol^{-1}) of $(U_{0.80}Pu_{0.20})O_2$, the line represents the results of the calculation presented in this work, ○ show the experimental data from Ogard [26] for O/(U + Pu) = 2.00, ◇ show the experimental data from Ogard [26] for O/(U + Pu) = 1.98 and △ the experimental data from Leibowitz et al. [27] for O/(Pu + Pu) = 1.97.

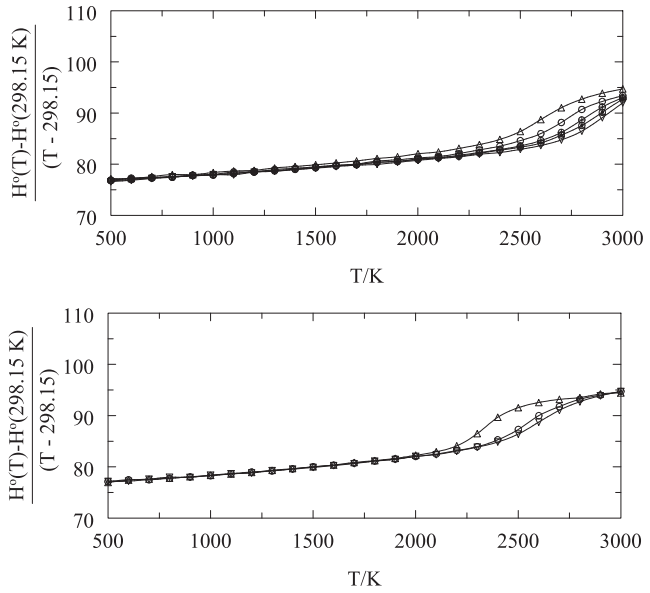

Fig. 6. The reduced enthalpy increment (in J K−1 mol^{-1}) of $(Th_{1-x}\ U_x)O_2$ for $x = 0.08$, 0.15 and 0.30 (top) and $(U_{1-x}\ Pu_x)O_2$ for $x = 0.20$ (bottom). The solid lines represents the results of the MD calculations using the CRG potential.

The same observation is made for the $(U_{0.80}Pu_{0.20})O_2$ solid solution, though the overall agreement is less than for $(Th_{1-x}U_x)O_2$. This may be explained due to the lower PuO_2 reduced enthalpy in the Debye region that was predicted by the CRG potential compared to the experiment. Despite the high-temperature Bredig transition predicted by the model for UO_2, PuO_2 and (U,Pu)O_2 [5] it is not sufficient to compensate for the low prediction of reduced enthalpy at intermediate temperatures. Note that in the original CRG paper the PuO_2 heat capacity was predicted to be relatively constant [3], however this is thought to be an artifact of the polynomial form used in the analysis and the later more rigorous investigation using this potential exhibits the Bredig transition [5].

Although Fig. 6 indicates differences between the experiment and MD calculations particularly for the lattice contribution in the Debye region, it shows that in the high-temperature regime the onset temperature for excess enthalpy and heat capacity are in qualitative agreement. Addition of U to ThO_2 (see Fig. 6a) reduces the temperature at which excess heat capacity occurs, in line with the results reported in Fig. 4. However, the effect of adding U to ThO_2 is more significant for the MD results than for the analytical model. This can be explained by considering that there exist a wide range of unique oxygen environments in our MD simulations that arise due the random distribution of actinides on the cation sublattice. Consequently, for a given actinide composition there is a probability distribution associated with the OFP energy. These distributions have been examined previously [4,5], indicating a skew towards OFP energies that are lower in the mixed systems than the linear interpolation of the end members. The treatment for the OFP energy in equation (1) does not account for this. Nonetheless, without a more detailed examination of cation distribution at the atomic scale it is not clear which approach is best suited to describing real mixed systems. Fig. 6b shows that additions of Pu to UO_2 also reduce the temperature at which excess heat capacity is predicted by MD. Although the absolute values for reduced enthalpy are not in agreement, this temperature shift for excess enthalpy in $(U_{0.80}Pu_{0.20})O_2$ is in line with the prediction made using the analytical model and the experimental data.

It should be remarked that the OFP concentrations calculated by the analytical Szwarc model and the MD calculations are in fair agreement: the fraction rises up to 0.01 to 0.05 near the melting temperature for the analytical model, depending on the Pu concentration, and up to 0.03 for the MD calculations in the region below the Bredig transition (this transition prevents calculating concentrations at higher temperatures). These values are somewhat lower than those found in high-temperature neutron diffraction studies, which show that the defect concentration increases to 0.15 near the melting [35].

5. The pre-melting region: the effect of oxygen point defects

Finally, we checked for the effect of oxygen point defects caused by changes in the composition at very high temperature (premelting) related to the reduction of the dioxide to a slightly substoichiometric phase. Calculations were performed for $(U_{0.80}Pu_{0.20})O_2$ with the ThermoCalc Software using the database for the U-Pu-O system from the assessment by Guéneau et al. [36]. The calculation was simulating the capsule design and dimension from the paper by Ogard [26], for a constant volume corresponding to the free volume and an Ar gas atmosphere (0.33 atm). The calculation showed that equilibrium between the $(U_{0.80}Pu_{0.20})O_2$ sample and the gas phase leads to a very small deviation from the initial stoichiometry at very high temperature (δ(O/M) <0.0025 at 3000 K for initial O/(U + Pu) = 2.00 as shown in Fig. 7, and δ(O/M) < 0.0225 for at 3000 K for initial O/(U + Pu) = 1.98), with no significant impact of the related oxygen point defects on the heat capacity. It should be noted here that in an open system, the effect would be more pronounced.

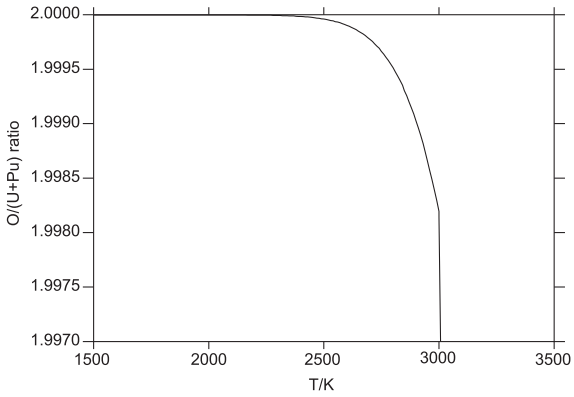

Fig. 7. The O/(U + Pu) ratio as a function of temperature as obtained from thermodynamic simulation of the drop calorimetric experiment for of $(U_{0.80}Pu_{0.20})O_2$ by Ogard [26].

6. Discussion and conclusions

The current analysis can be combined with recent results concerning the heat capacity of the (Th,Pu)O_2 solid solution, for which measurements were made in the low-temperature regime (4–300 K) [37] and the intermediate regime (400–1700 K) [38] to obtain a clear picture in the widest possible temperature range.

The low-temperature heat capacity measurements for the (Th,Pu)O_2 solid solution have shown that below 30 K an effect of cation substitution is clearly observable. In absolute sense the heat capacity of the mixed oxide solutions is systematically above that of the end members, in relative sense the excess reaches 50% of the lattice heat capacity, calculated from the end members by the additivity rule (NK rule) at the lowest temperatures and quickly decreases with increasing temperature, approaching values close or just above those obtained from the NK rule. This is caused by cation substitutional disorder in the crystal leading to phonon scattering as a result of lattice strain. This is highly dependent on the differences in the size of the substitutional atoms, which are the largest in (Th,Pu)O_2 solid solution when considering actinide dioxides. It is expected to be less pronounced in the (Th,U)O_2 and (U,Pu)O_2 solid solutions, but experimental data to confirm this are lacking.

In the intermediate temperature range, the experimental enthalpy increments data from literature sources and obtained in our laboratory for (Th,Pu)O_2, (Th,U)O_2 and (U,Pu)O_2 show no deviations from the NK rule and yield heat capacity values close to the Dulong-Petit limit of 6*R*.

The available literature data in the high temperature range for enthalpy increments show an excess heat capacity contribution that can be described well by Szwarc's model for OFP in fluorite dioxides. We have shown that by linear interpolation of the enthalpies and entropies of oxygen Frenkel pair formation for the end-members, as derived by us in earlier work [1], the experimental enthalpy data can be described quite accurately. In principle this interpolation yields results that are close to those obtained by the additivity rule, but with more firm physical basis. These data are, however, not in agreement with the results of many-body potential model calculations that clearly show the contribution of the Bredig transition to the enthalpy.

The Bredig (superionic) transition has been reported by Hiernaut et al. [23] for UO_2 and by Ronchi and Hiernaut [24] for ThO_2 and has been explained by order-disorder displacement on the

anion site, with the maximum disorder occurring at the transition. Its existence was derived from thermal arrests in cooling curves for laser-heated samples, but was strongly dependent on the gas atmosphere. Neutron scattering measurements by Hutchings [39] gave evidence for thermally induced Frenkel oxygen lattice disorder at temperatures >2000 K in UO_2 and ThO_2, with the total of defective anions steadily increasing to approximately 30% at T = 2930 K. A recent synchrotron X-ray study also indicated substantial oxygen disorder in UO_2 in the temperature range of the Bredig transition [40], with increasing U-U distance with temperature, in agreement with lattice expansion, but decreasing U-O distance. The authors found a good agreement with the results of the molecular dynamics study by Yakub et al. [41] that showed the Bredig (superionic) transition at around 2700 K.

According to the CRG calculations the enthalpy effect of the Bredig (superionic) transition is substantial, of the order of 30 kJ mol^{-1} (Figs. 4 and 5) and although it is diffuse, the magnitude is such that it should have been detected in the enthalpy increment measurements by Refs. [25–27] as an inflection. It could be argued that the during the enthalpy drop measurements the disordered state is quenched and that the measurements do not refer to the ideal crystal but to a disordered end state. This is, however, not likely because in the laser heating measurements by Hiernaut and Ronchi [23,24] very fast quenching was applied also, faster than the calorimetric measurements, and the energy release of the restructuring to the ordered state was observed as a clear thermal arrest. Our recent measurements performed on laser melting and quenched ThO_2, UO_2, and PuO_2 samples [12,42–44] show neither a thermal arrest nor quenching of a highly disordered crystal structure, which should be visible by X-ray diffraction and Raman spectroscopy. It is thus not straightforward to reconcile the experimental results.

A possible explanation should be sought in defect types and energetics. It is well known that defect clustering occurs in UO_2 [13] and that the concentration of such clusters increases with temperature, where the mobility of point defects increases. In this context the configurational entropy of point defects and small clusters must also be considered. This quantity has been shown to be surprisingly large in strongly defected solids, leading to significant corrections to the free energies of defect clusters at high temperatures [45]. Another factor is that there does not exist just one OFP energy in the solid solution but rather there are a wide range of possible oxygen environments depending on the local actinide coordination. Moreover, considering the high concentration of defects at high temperatures, a concentration and hence a temperature dependence of the defect formation energies should be considered. In the Szwarc's model this is not accounted for and the OFP energy obtained from that model must be considered as an "effective" energy. We hypothesize here that such energetic differences can lead to a shift of the Bredig (superionic) transition to higher temperature, as a result of which the maximum of the disordering could occur upon melting and not before.

Acknowledgements

The authors wish to acknowledge to support of J. Somers and his colleagues for providing the samples, and O.S.V. acknowledges the European Commission support for his research fellowship. Computational resources are due to the Imperial College High Performance Computing Service.

References

[1] R.J.M. Konings, O. Beneš, J. Phys. Chem. Solids 74 (2013) 653–655.
[2] K. Popa, R.J.M. Konings, T. Geisler, J. Chem. Thermodyn. 39 (2006) 236–239.
[3] M.W.D. Cooper, M.J.D. Rushton, R.W. Grimes, J. Phys. Condens. Matter 26 (2014) 105401.
[4] M.W.D. Cooper, S.T. Murphy, P.C.M. Fossati, Michael, J.D. Rushton, R.W. Grimes, Proc. R. Soc. A 470 (2014) 20140427.
[5] M.W.D. Cooper, S.T. Murphy, M.J.D. Rushdon, R.W. Grimes, J. Nucl. Mater 461 (2015) 206–214.
[6] D. Sedmidubský, O. Beneš, R.J.M. Konings, J. Chem. Thermodyn. 37 (2005) 1098–1103.
[7] S. Hubert, J. Purans, G. Heisbourg, P. Moisy, N. Dacheux, Inorg. Chem. 45 (2006) 3887–3894.
[8] R.J.M. Konings, O. Beneš, A. Kovács, D. Manara, D. Sedmidubský, L. Gorokhov, V.S. Iorish, V. Yungman, J. Phys. Chem. Ref. Data 43 (2014) 013101.
[9] S. Anthonysamya, J. Joseph, P.R. Vasudeva Rao, J. Alloys Comp. 299 (2000) 112–117.
[10] R. Kandan, R. Babu, P. Manikandan, R. Venkata Krishnan, K. Nagarajan, J. Nucl. Mater 384 (2009) 231–235.
[11] F. De Bruycker, K. Boboridis, P. Pöml, R. Eloirdi, R.J.M. Konings, D. Manara, J. Nucl. Mater 416 (2011) 166–172.
[12] R. Böhler, M.J. Welland, D. Prieur, P. Çakir, T. Vitova, T. Pruessmann, I. Pidchenko, C. Hennig, C. Guéneau, R.J.M. Konings, D. Manara, J. Nucl. Mater 448 (2014) 330–339.
[13] C. Guéneau, A. Chartier, L. Van Brutzel, in: R.J.M. Konings, T. Allen, R. Stoller, S. Yamanaka (Eds.), Comprehensive Nuclear Materials vol. 2, Elsevier, 2012 (Chapter 2).02.
[14] R.L. Gibby, Hanford Engineering Development Laboratory, Technical Report HEDL-TME-73-19, 1973.
[15] R. Kandan, R. Babu, K. Nagarajan, P.R. Vasudeva Rao, J. Nucl. Mater 324 (2004) 215–219.
[16] R. Kandan, R. Babu, K. Nagarajan, P.R. Vasudeva Rao, Thermochim. Acta 472 (2008) 46–49.
[17] R. Szwarc, J. Phys. Chem. Solids 30 (1969) 705–712.
[18] C. Wagner, W. Schottky, Z. phys, Z. Chem Bll, Phys. Chem. B 11 (1931) 163.
[19] J.K. Fink, J. Nucl. Mater 279 (2000) 1–18.
[20] R.J.M. Konings, M. Bertolus, in: J. Gibson, W. de Jong (Eds.), Behaviour and Properties of Nuclear Fuels, Wiley Publishers, 2017 (Chapter 6).
[21] E. Vathonne, J. Wiktor, M. Freyss, G. Jomard, M. Bertolus, J. Phys. Condens. Matter 26 (2014) 325501.
[22] R. Ngayam-Happy, M. Krack, A. Pautz, J. Phys. Condens. Matter 27 (45) (2015) 455401.
[23] J.P. Hiernaut, G.J. Hyland, C. Ronchi, Int. J. Thermophys. 14 (1993) 259–283.
[24] C. Ronchi, J.P. Hiernaut, J. Alloys Comp. 240 (1996) 179–185.
[25] D.F. Fischer, J.K. Fink, L. Leibowitz, J. Belle, J. Nucl. Mater 118 (1983) 342–348.
[26] A.E. Ogard, J.A. Leary, Thermodynamics of Nuclear Materials 1967, International Atomic Energy Agency, Vienna, 1968, p. 651.
[27] L. Leibowitz, D.F. Fischer, M.G. Chasanov, J. Nucl. Mater 42 (1972) 113–116.
[28] S. Plimpton, J. Comp. Phys. 117 (1995) 1–19.
[29] R.A. Buckingham, Proc. Roy. Soc. Lond A 168 (1938) 264–283.
[30] P. Morse, Phys. Rev. 34 (1929) 57–64.
[31] P.P. Ewald, Ann. Phys. 369 (1921) 253–287.
[32] R.W. Hockney, J.W. Eastwood, Computer Simulation Using Particles, Adam Hilger, New York, NY, 1988.
[33] M.S. Daw, M.I. Baskes, Phys. Rev. B 29 (1984) 6442–6453.
[34] M.W.D. Cooper, Atomic Scale Simulation of Irradiated Nuclear Fuel, PhD Thesis, Imperial College London, 2015 (http://ethos.bl.uk/OrderDetails.do?uin=uk.bl.ethos.650725).
[35] K. Clausen, W. Hayes, J.E. Macdonald, R. Osborn, Phys. Rev. Lett. 52 (1984) 1238–1241.
[36] C. Guéneau, N. Dupin, C. Martial, J. C Dumas, S. Gossé, S. Chatain, B. Sundman, F. De Bruycker, D. Manara, R.J.M. Konings, J. Nucl. Mater 419 (2011) 145–167.
[37] S.O. Vălu, O. Beneš, R.J.M. Konings, J.C. Griveau, E. Colineau, J. Phys. Chem. Solids Submitt. 86 (2014) 194–206. November 2015.
[38] S.O. Vălu, D. Staicu, O. Beneš, R.J.M. Konings, P. Lajarge, J. Alloys Comps 614 (2014) 144.
[39] M.T. Hutchings, J. Chem. Soc. Faraday Trans. II 83 (1987) 1083–1103.
[40] L.B. Skinner, C.J. Benmore, J.K.R. Weber, M.A. Williamson, A. Tamalonis, A. Hebden, T. Wiencek, O.L. Alderman, M. Guthrie, Leibowitz, J.B. Parise, Science 346 (2014) 984–987.
[41] E. Yakub, C. Ronchi, D. Staicu, J. Chem. Phys. 127 (2007) 094508.
[42] D. Manara, C. Ronchi, M. Sheindlin, High. Temp.-High Press 35/36 (2003) 25–33.
[43] D. Manara, C. Ronchi, M. Sheindlin, M. Lewis, M. Brykin, J. Nucl. Mater 342 (2005) 148–163.
[44] F. De Bruycker, K. Boboridis, D. Manara, P. Pöml, M. Rini, R.J.M. Konings, Mater. Today 13 (11) (2010) 52–55.
[45] S.S. Kapur, M. Prasad, J.C. Crocker, T. Sinno, Phys. Rev. B 72 (2005) 014119.